

COVER PAGE

Document downloaded by @DAEL

Thu Nov 26 17:28:44 2026
For personal use

When automatic English translation is provided, only the original document is authentic.
The EAA cannot be held responsible of any translation error

Bibliographical reference

The Reflection Map: A New Tool for Frequency to Time Domain Study of 1D Acoustical Systems, S. Rodriguez, V. Gibiat, S. Guilain and A. Lefebvre, Acta Acustica **vol. 95** (Number 5), 2009, pp. 795-804

DOI
https://doi.org/10.3813/AAA.918210

Acta Acustica united with Acustica
Vol. 95 (2009) 795 – 804

DOI 10.3813/AAA.918210

The Reflection Map: A New Tool for Frequency to Time Domain Study of 1D Acoustical Systems

S. Rodriguez[1)], V. Gibiat[2)], S. Guilain[1)], A. Lefebvre[1)]

[1)] Renault, Centre technique de Lardy, CTL L16 1 29, 1 allée Cornuel, 91510 Lardy, France. [samuel.rodriguez; stephane.guilain; alain.a.lefebvre]@renault.com

[2)] Laboratoire PHASE (EA 3028), Université Paul Sabatier, 118, route de Narbonne 31 062 Toulouse Cedex 9, France. gibiat@cict.fr

Summary

The time domain determination of the impulse response, or the reflection function of an acoustical system from data expressed in the frequency domain, is not immediate. Signal processing from frequency domain to time domain may involve non physical phenomena of large amplitude as unphysical oscillations known as "ripple". Signal processing techniques based on filtering in the frequency domain are often used to limit or remove this ripple. These techniques involve modifications on the original data and on the resulting time domain function. The aim of this study is to present a new tool to avoid such modifications: The reflection map. Its use combined with a new observable directly obtained from the reflection function, the integrated squared reflection function, allows a minimization of the ripple phenomenon that we show is impossible to eliminate except for a cylindrical tube.

PACS no. 43.20.Mv, 43.58.Gn, 43.60.Pt

1. Introduction

Frequency domain is helpful to understand several physical phenomena. However, the time domain can be very useful if the duration of the function is short enough to be easily analyzed. In duct acoustics it can give information about the geometry. It provides useful tools for exploring bore reconstruction of musical instruments, for which previous important studies have been done [1, 2]. In addition, the results obtained for musical instruments can be directly applied to specific engine applications; acoustic resonances in intake and exhaust systems are crucial for the performances of the engine [3]. For both musical systems and engines, measurements and simulations are very often performed in the frequency domain, but their transcriptions in the time domain are essential for physical interpretation and industrial applications.

McIntyre *et al.* [4] defined the reflection function as the disturbance that would be at the abscissa x after the delta-function pulse is sent out, if the tube was terminated at x by a perfect absorber. Previous works of Gazengel *et al.* [5], for applications in musical synthesis, have shown that the misuse of impedance $Z(\omega)$ (with $\omega = 2\pi f$ the pulsation and f the frequency) in order to obtain the reflection function leads to spurious oscillations in time domain called ripple. These oscillations are difficult to separate from physical oscillations deriving, for example, from trapped waves between two closed section discontinuities. They are also different and difficult to separate from Gibbs phenomena. It is worth pointing out that the Gibbs phenomenon arises when approximating a discontinuous function by a finite series of continuous sine and cosine waves. In some simple cases, the ripple can also be understood as the result of a discontinuity on the windowed impedance. However it is not always the case, as explained in section 4.2. Various solutions have been presented to limit the ripple leading to divergent numerical solutions in physical modelling of musical instruments [5]. The rotation of phase and the application of a low pass filter are among them. Following Shannon's rule, the authors of [5] showed that the sampling frequency had to be chosen equal to $2F_{\max}$ ($F_{\max}$ is the maximum frequency of the input impedance), with $F_{\max}$ corresponding to a maximum of the impedance magnitude. This solution appeared to be quite efficient.

In a second paper, Amir *et al.* [6] proposed an all pole filtering model that is most efficient for a single reflection system. These solutions are clearly signal processing ones and do not indicate anything about the physical behaviors that govern the acoustical system.

For a cylindrical tube, Polack *et al.* have analytically determined [7] the time domain expression of a reflection function. Propagation with visco-thermal losses in the time domain have also been modeled by Helie and al. [8] with fractional calculus, but those mathematical tools are beyond the scope of this paper.

Received 26 September 2007,
accepted 8 May 2009.

© S. Hirzel Verlag · EAA

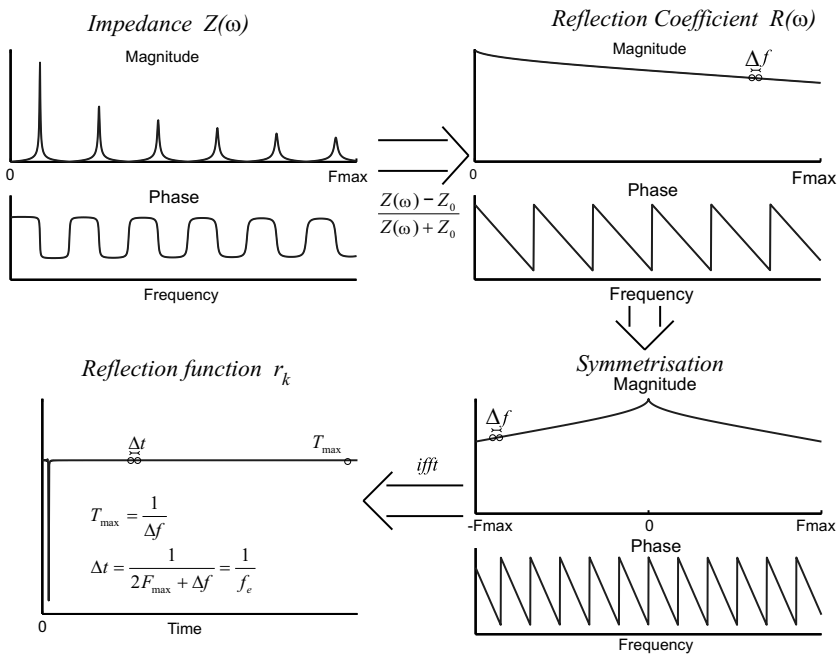


Figure 1. From impedance to reflection function in three steps.

After a detailed presentation of the numerical computation and a discussion on the analytical solution of Polack *et al.* in II), the reflection function of a cylindrical duct is carefully studied in III). A ripple minimization technique is demonstrated. The integrated squared reflection function is introduced and applied on measurements of an air intake system. Section 4 deals with the reflection function of a two reflections system. The reflection map is introduced in the last section. Reflection functions of a system are computed for a set of different frequency domains. The reflection map represents this whole set of functions on a unique graphic, where a ripple free line can be often drawn. The reflection map appears to be a new tool for extracting physical information from reflection functions.

2. From impedance to reflection function

2.1. Numerical approach

The reflection function $r(t)$ is the inverse Fourier Transform of the reflection coefficient

$$R(\omega) = \frac{Z(\omega) - Z_0}{Z(\omega) + Z_0}, \tag{1}$$

that is obtained from the impedance $Z(\omega) = X(\omega) + \mathrm{i}Y(\omega)$ with the characteristic impedance of the medium.

If the frequency domain is continuous, the reflection function is defined as

$$r_{\mathrm{an}}(t) = \int_0^{\infty} R(\omega) H_{F_{\max}}(\omega) \mathrm{e}^{\mathrm{i}\omega t} \mathrm{d}\omega, \tag{2}$$

where

$$H_{F_{\max}}(\omega) = \begin{cases} 1 & \text{for } \omega \in [0, 2\pi F_{\max}], \\ 0 & \text{otherwise.} \end{cases}$$

On the discrete frequency and time domains, the reflection function is defined as

$$\begin{aligned} r_k &= \mathrm{DFT}^{-1}\left(R_{[-\omega_N, \omega_N]}(\omega)\right) \\ &= \frac{1}{2N+1} \sum_{l=-N}^{N} R\left(2\pi F_{\max} \frac{l}{N}\right) \\ &\quad \cdot \exp\left(\mathrm{i}2\pi F_{\max} \frac{l}{N} \frac{k}{f_e}\right), \end{aligned} \tag{3}$$

$k = 0 : 1 : 2N$, with N the number of samples in the discrete reflection coefficient $R(\omega)$, and

$$R_{[-\omega_N, \omega_N]}(\omega) = \left[R^*(-\omega) R(0) R(\omega)\right],$$

where $R(0)$ is the average value of the reflection function.

The reflection function represents, as defined in McIntyre *et al.* [4], the pressure response of the duct to an impulse, assuming that the plane where the impulse is produced and where the measure is done is preceded by an anechoic termination as a matched impedance. It drastically limits the duration of the function, compared to the impulse response obtained as the inverse Fourier Transform of the impedance.

The process to calculate r_k is summarized in Figure 1. As the direct Fourier Transform is today of common use, its properties and drawbacks have been well studied. Its main properties can be found for example in [9] and for $X(\omega)$ the Fourier Transform of the real signal $x(k)$, $X(-\omega) = X^*(\omega)$.

In the frequency domain, these properties have to be verified in order to obtain, through the inverse Fourier Transform, a result that carries physical information. As an example, a physical result in the time domain is necessarily a real value. The "symmetrisation" step, described in Figure 1, provides such a result through the inverse Fourier

Transform. The "symmetrisation" produces $2N + 1$ samples from N samples. The N samples are mirrored and the central value, corresponding to frequency 0, is added.

The frequency domain models do not predict the value at 0 Hz. The physical meaning of $R(0\,\text{Hz})$ is the mean value of r_k. A random real value is first chosen for $R(0\,\text{Hz})$, then r_k is computed. It is reasonable to consider that r_k quickly decays with time and that the mean value of the last samples should be 0. If it is not the case, the mean value of the last samples is subtracted to all r_k.

For example, if $f_e = 10001\,\text{Hz}$ and $\Delta f = 1\,\text{Hz}$, the symmetrized R is composed of 10001 elements, from $-5000\,\text{Hz}$ to $5000\,\text{Hz}$, including 0 Hz (or from 0 to 10000 Hz as the Discrete Fourier Transform is periodic). The original R (before the symmetrization) is composed of 5000 elements, from 1 to 5000 Hz. If $f_e = 10000\,\text{Hz}$ is preferred, there are 10000 elements in the symmetrized R, from -4999 to 5000 Hz (or from 0 to 9999 Hz), and the real value of $R(5000\,\text{Hz})$ replaces $R(5000\,\text{Hz})$. One avoids this small change with $f_e = 10001\,\text{Hz}$ rather than 10000 Hz, as suggested by the symmetrization method. Anyway the results are not dramatically affected.

Numerically, the impedance is given in a discrete frequency domain from Δf to $F_{\max}$ with a Δf step; the time interval Δt between two points in the dual time domain after the inverse Fourier Transform is given by

$$\Delta t = \frac{1}{2F_{\max} + \Delta f} = \frac{1}{f_e}. \tag{4}$$

The time needed for the wave to go back and forth to the first reflective condition (section discontinuity for instance) is measured on the time axis at the first peak. As time is proportional to the distance with the hypothesis of a constant celerity of sound wave c, the distance Δx between the measured impedance and the impedance discontinuity responsible for the reflection is therefore given by

$$\Delta x = \frac{c\,\Delta t}{2}. \tag{5}$$

For a known wave speed c, a time sampling is equivalent to a spatial sampling

$$\Delta x_e = \frac{c}{2f_e}. \tag{6}$$

With $f_e = 10001$ Hz (it means, the impedance is measured or simulated from 1 up to 5000 Hz) and $c = 346$ m/s, $\Delta x = 17.3$ mm.

The natural way to increase the spatial accuracy is to increase the sampling frequency. Mathematically speaking, it is true. It is equivalent to increasing the upper limit of the frequency domain. Nevertheless, in a cylindrical tube, the impedance is only defined for frequency below the first cut-off frequency of the tube. It imposes a physical frequency limit, the cause of a limited spatial resolution. Increasing the sampling frequency does not provide more accuracy when $F_{\max}$ becomes higher than the first cut-off frequency of the acoustical system. For frequency higher than the cut-off frequency, information becomes meaningless, at least in a plane wave model. Extending the frequency range with zero values only leads to a non-physical interpolation. One consequence is that it will never be well-described, as the peak of the reflection function is often a very short event. It is of great importance for many applications as for bore reconstruction [1, 2], discontinuities detections [10], etc.

As analytical results are available, the problems occurring in this kind of numerical determination can be observed on a cylindrical tube, as well as on multiple reflection systems.

2.2. Analytical approach

The previous section deals with the numerical integration of the inverse Fourier Transform leading to the time domain reflection function r_k. To our knowledge, there is only one analytical expression of such a reflection function in the case of a cylindrical tube that has been derived by Polack *et al.* [7]. This analytical expression includes thermal and viscous losses at walls but neglects the radiation losses and gives for an open cylindrical duct

$$\begin{aligned} r_{\text{an}}(t) &= -\frac{A}{\sqrt{\pi}} f\left(t-\tau, A\right) \qquad (7)\\ f\left(t-\tau, A\right) &= 0, \qquad t \le \tau,\\ f\left(t-\tau, A\right) &= \frac{\mathrm{e}^{-A^2/(t-\tau)}}{(t-\tau)^{3/2}}, \qquad t > \tau, \end{aligned}$$

where A is related to the visco-thermal losses, and τ to the propagation time (more details are provided in [7] and are beyond the scope of this paper).

This result has three important drawbacks. First, the radiation losses are neglected. Second, the integration on the whole frequency domain implies that the plane wave hypothesis and the models for visco-thermal losses and radiation are efficient for all frequencies. The two previous elements have a consequence; the analytical solution of Polack *et al.* is suitable only for long and thin ducts. Finally, the amplitude of the analytical solution does not have any immediate and obvious physical meaning, as the reflection coefficients do. As a matter of fact, the results of [7] have an amplitude of $-60\,\text{s}^{-1}$, as the ones obtained with the numerical results are between -1 and 1, and are dimensionless, since they correspond to a ratio between the outgoing and the incoming pressures.

3. Reflection function of a cylindrical tube

Gazengel *et al.* [5], and Amir *et al.* [6] presented results and solutions to eliminate the ripple. They have not given any explanation about its physical or mathematical origins. Using similar examples, it is possible to give an explanation of the ripple.

3.1. Ripple minimization technique

The first example is a 1 m long cylindrical pipe of inner radius of 15 mm with an open unflanged end. The impedance

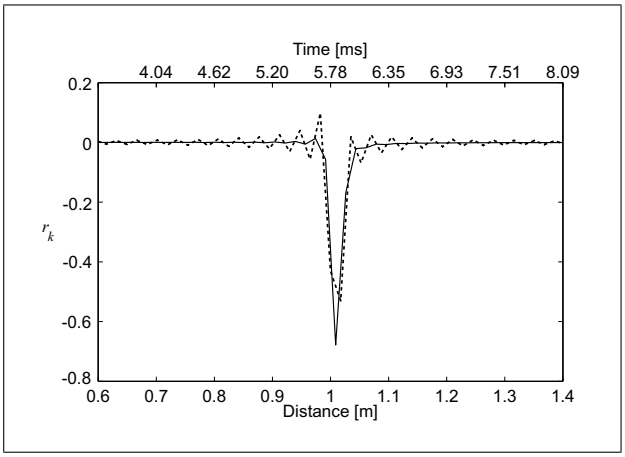


Figure 2. Reflection function of a 1 m cylindrical pipe. The diameter is 30 mm.
Solid line: $F_{\max} = 4976\,\text{Hz}$; $\theta(f = F_{\max} 4976\,\text{Hz}) \approx -\pi$;
Dashed line: $F_{\max} = 4934\,\text{Hz}$; $\theta(f = F_{\max} 4934\,\text{Hz}) \approx -\pi/2$.

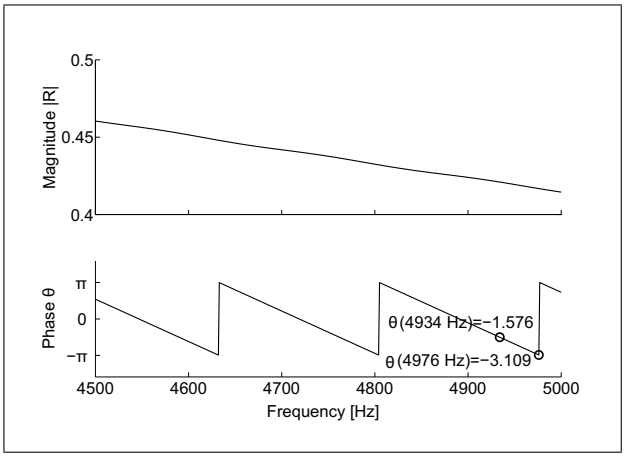


Figure 3. Reflection coefficient of the 1 m cylindrical pipe. The observable is zoomed between 4500 and 5000 Hz.

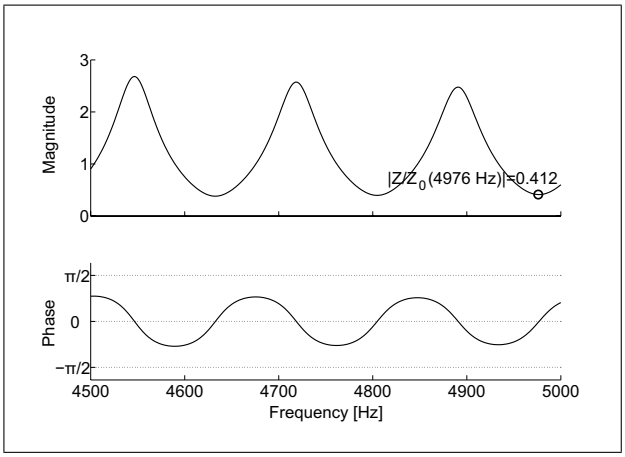


Figure 4. Normalised impedance of the 1 m cylindrical pipe. The observable is zoomed between 4500 and 5000 Hz.

is easily computed with a 1D classical acoustic model that takes into account the visco-thermal losses in frequency domain [11] as well as the radiation through the Levine and Schwinger model [12]. The reflection coefficient $R(\omega)$ is then computed from 1 up to 5000 Hz with $\Delta f = 1\,\text{Hz}$. The value at 0 Hz is the average value of the time domain function. As $R(\omega)$ is a complex function, it can be written $||R(\omega)||\text{e}^{\text{i}\theta(\omega)}$.

The reflection function is obtained through a Fast Fourier Transform algorithm. A simple rectangular window is chosen so that the integrity of the original signal is kept. The window is extended from $-F_{\max}$ up to $F_{\max}$. The only difference between the two reflection functions presented on Figure 2 is the value of the upper limit of the frequency domain $F_{\max}$. In the first case, the data is kept up to 4976 Hz. In the second case, it is kept up to 4934 Hz (dashed line). The two $F_{\max}$ values were chosen so that the phase of the reflection coefficient on Figure 3 verifies

$$\theta(F_{\max}) = 0(\text{mod}\pi) \Leftrightarrow Y(F_{\max}) = 0 \tag{8}$$

in the first case and $\theta(F_{\max}) = \pi/2(\text{mod}\pi)$ in the second case. The result is nearly free of ripple in the first case. The other case is beset by ripple and the peak is poorly defined. It means that the time sampling is not compatible with the exact position of the peak as the spatial sampling Δx_e does not match the physical geometry.

Imposing a zero phase of the reflection coefficient at $F_{\max}$ yields destructive interferences out of the peak region. But imposing another value yields constructive interferences. A value of $\pi/2$ has a consequence of a strong ripple. It is worth to point out that Gazengel *et al.* [5] gave a solution that does not fulfil our condition. Moreover the sentence "If $F_{\max}$ is chosen to be on a zero of $|Z(f)|$, $r_d[n]$ is beset by ripple, [...] whereas if $F_{\max}$ is chosen to be equal to a resonance frequency of $Z(f)$ defined by $\Im m\{Z(f)\} = 0$, where $\Im m$ represents the imaginary part, this ripple nearly disappears." extracted from [5] proposes a value of $F_{\max}$ (the one so that $Z(F_{\max})$ is minimum) that should lead to ripple. Our example shows it is not sufficient (as claimed by the authors of [5] in their conclusion). This assumption will be demonstrated thanks to the reflection map in V). The value of 4976 Hz yields a ripple free solution and corresponds to a minimum of the modulus of the impedance. (Figure 4)

Two abscissa axes are used in Figure 2. One is a classical time axis, the other one is a distance axis as defined in (5). It is half the distance run by the wave during the corresponding time. This double axis will be used in every plot depending on time.

3.2. The integrated squared reflection function

An important point is the relationship between the bad determination of the peak maximum and the ripple.

The energy of a signal r_k is given by

$$E_r = \frac{1}{f_e} \sum_{k=1}^{N} r_k^2. \tag{9}$$

The Parseval theorem yields

$$E_r = \frac{1}{N f_e} \left(R(0)^2 + 2 \sum_{k=0}^{N/2-1} \left| R(k) \right|^2 \right), \tag{10}$$

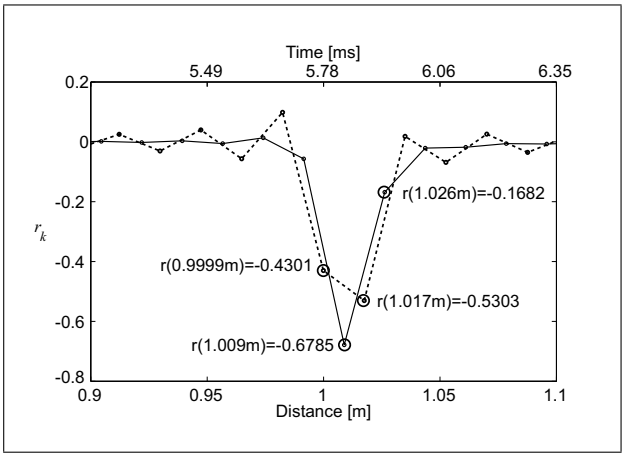


Figure 5. Reflection function of a 1 m cylindrical pipe. The diameter is 30 mm. Solid line: $F_{\max} = 4976$ Hz; Dashed line: $F_{\max} = 4934$ Hz.

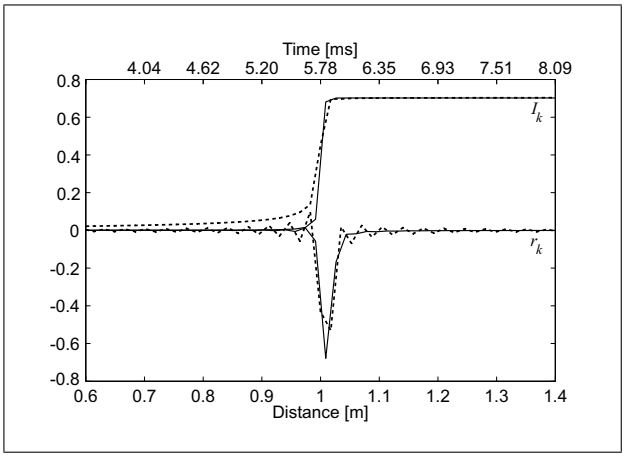


Figure 6. Reflection function and integrated squared reflection function of a 1 m cylindrical pipe. The diameter is 30 mm. Solid line: $F_{\max} = 4976$ Hz; Dashed line: $F_{\max} = 4934$ Hz.

where $R(k)$ is the Fourier Transform of r_k; the energy is a sum of squared discrete values. Two of these discrete values are chosen for each result on Figure 5. They best describe the peak of each reflection function. The application of (9) on each case is limited to the two points describing the reflection in order to estimate the energy concentration caused by the peak. On one hand, the energy concentration is $(0.4301^2 + 0.5353^2)/\sum_k r_k^2 \approx 0.94$. On the other hand, it is $(0.6785^2 + 0.1682^2)/\sum_k r_k^2 \approx 0.99$. The two chosen points of the rippled signal contain 94% of the total energy, while they contain 99% of the total energy of the ripple free reflection function. The missing energy is transferred to the ripple, as a mathematical consequence of Parseval's theorem.

The energy concentration can be graphically illustrated with a new observable: the integrated squared reflection function, defined by

$$I_n = \sum_{k=1}^{n} r_k^2, \tag{11}$$

where n corresponds to the nth sample of r_k. It represents the accumulation of energy with respect to time. As clearly visible on Figure 6, the reflection phenomenon is highlighted, compared with the ripple that besets r_k. This kind of variable has proved to be very useful for complex geometries, especially for measurements.

A practical interest of I_k is the geometrical study of an acoustical system composed of different elements. The first step is the acoustic characterization of the system's first element. The system is then measured every time a new element is added.

An air intake duct of a four-cylinder engine is measured in four different configurations with the TMTC method [13]. The system is composed respectively of A; A and B; A, B and C; A, B, C and D (Figure 7). Element A is composed of the primary ducts and the plenum (the volume common to all cylinders). B is a throttle. C is a duct with branch resonators. D is an air filter. The measurement system is connected to the intake at one of the

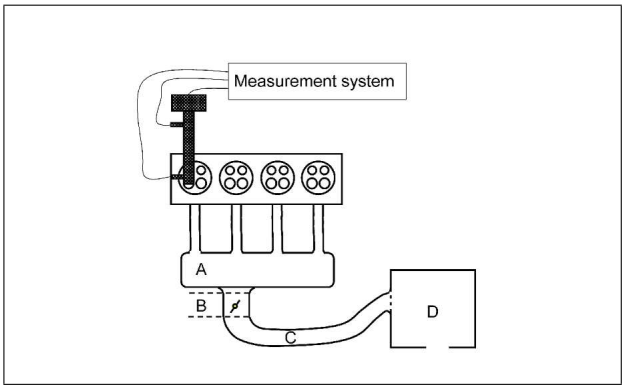


Figure 7. Air intake of a four-cylinder engine measured with the TMTC method.

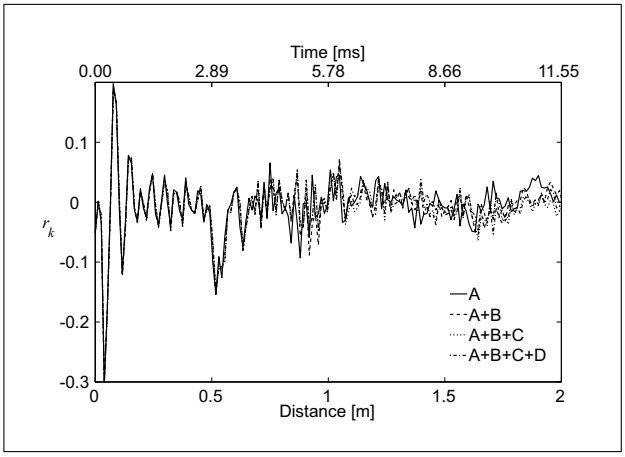


Figure 8. Reflection functions r_k of the four configurations of the system.

admission valve seats of one cylinder. As there are two admission valves per cylinder, the acoustic wave coming from the measurement system is reflected at the connection between the two small ducts of each valve. The closed end of the other valve also induces a reflection. These are the two reasons for the reflection functions' high ampli-

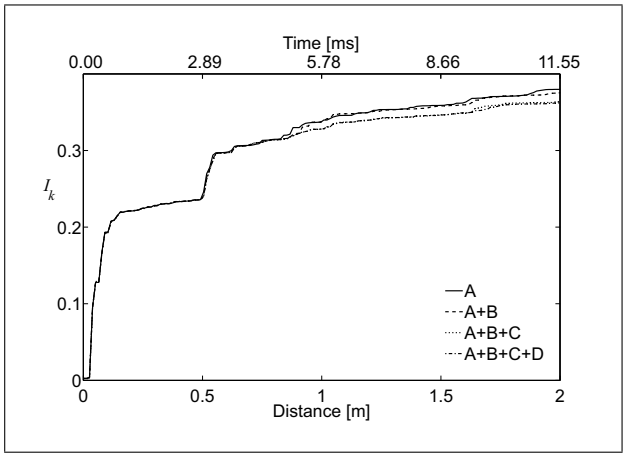


Figure 9. Integrated squared reflection functions I_k of the four configurations of the system.

tude value (Figure 8) during the first millisecond. The peak at 0.5 m corresponds to the junction between the primary duct and the plenum. The reflection functions are superimposed for distances smaller than 0.8 m, as are the integrated squared reflection functions (Figure 9). Below this value, no wave propagates further than the element A, and A belongs to all configurations. For higher distances (or propagation times), the reflection functions change. It becomes difficult to extract information about the geometry of the other elements. I_k allows to determine accurately where the system is changing with the amount of acoustic energy given back by the system. When adding element B to element A, the change occurs at 4.781 ms (or 0.8278 m). When adding C to A and B, it occurs at 5.2298 ms (or 0.9055 m). The difference of those two distances gives a measurement of the acoustical length of B: 77.7 mm. The real length of element B is 70 mm. When adding D to A, B and C, the change occurs at 9.4893 ms (or 1.643 m). The acoustic length of C is then 737.5 mm.

3.3. A filtering technique

The ripple appears as the expression of frequencies near to $f_e/2$. A natural signal processing solution to weaken these high frequencies would be to apply a weighting window; Figure 10a shows the application of such a window. However, a weighting window only limits the ripple as can be seen in Figure 10b. Moreover, the signal shape is modified and its total energy is reduced. As $F_{\max}$ is chosen to be 4934 Hz in both cases, the sampling frequency f_e does not match the physical events with or without the weighting window. Both reflection functions are beset by ripple and reflection peak's amplitude value is underestimated. As it modifies the results, no weighting window is used in what follows.

3.4. The ripple and the Gibbs phenomenon

The ripple phenomenon is different from the Gibbs phenomenon. The Gibbs phenomenon occurs when recomposing a signal with a discontinuity by a finite Fourier se-

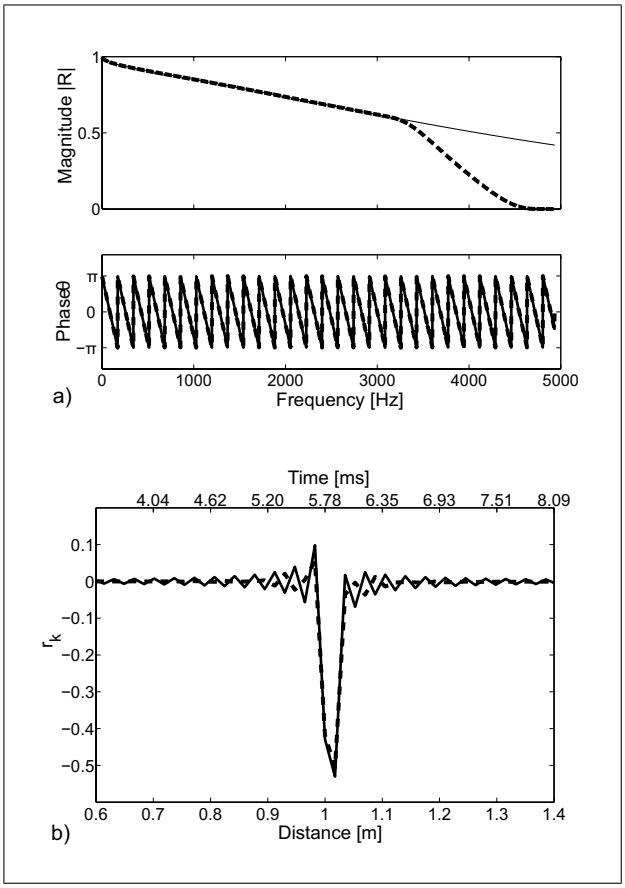


Figure 10. Reflection coefficient (a) and its corresponding reflection function (b) both with $F_{\max} = 4934$ Hz. Dashed line: with the weighting window; Solid line: without the weighting window.

ries [14]. The result is a sum of sinusoidal functions belonging to the interval $]-\infty;\infty[$. At the location of the discontinuity, the partial Fourier series converges to the midpoint of the jump, but there is an overshoot on one side of the discontinuity, and an undershoot on the other side. In a wider sense, the Gibbs phenomenon designates the sinusoidal variations at both sides of the discontinuity. These sinusoidal variations are due to the use of continuous sine and cosine waves. It is not the case here since the calculation of an inverse discrete Fourier Transform is the sum of time limited and discrete sinusoidal functions.

However, the Gibbs phenomenon can also be observed with the inverse discrete Fourier transform when doing zero-padding. This operation consists of completing the original signal with null values in order to increase the mathematical sampling frequency. It is equivalent to a sinusoidal interpolation in the dual domain for every base function. This interpolation is responsible for the sinusoidal oscillations characteristic of the Gibbs phenomenon.

4. Study of a multiple reflections system

Real acoustic systems, mufflers, air intake systems or musical instruments present many variations of geometry re-

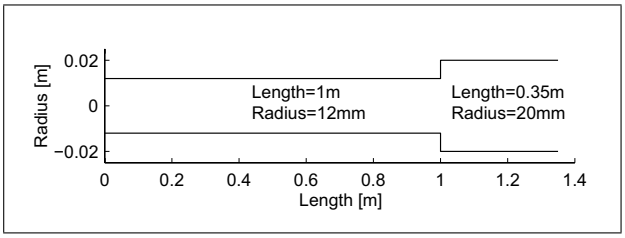


Figure 11. Geometry of the two-span system.

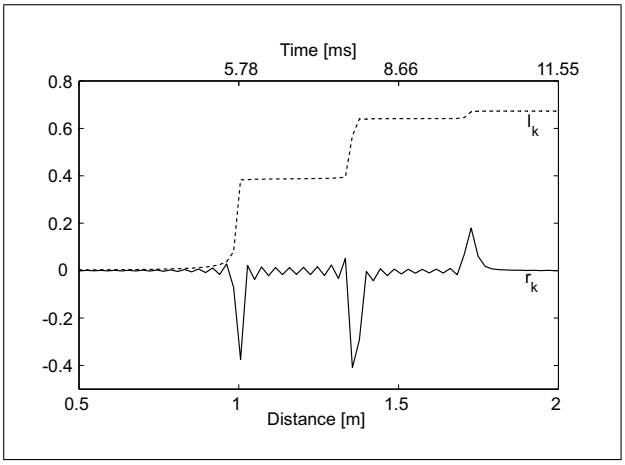


Figure 12. Reflection function and integrated squared reflection function of the acoustic line with $F_{\max} = 3959\,\text{Hz}$; $\theta(f = F_{\max} 3959\,\text{Hz}) \approx -\pi$.

sponsible for impedance discontinuities and complex reflection functions. Therefore, the case of a cylinder leading to a single reflection is quite restrictive. In real systems the time sampling would have to be compatible with the position of all the peaks; but, as the sampling frequency is constant with time, such a sampling frequency may not exist. In order to study the relationship between ripple and sampling, different values of $F_{\max}$ are tried.

The geometry of a more realistic example is shown in Figure 11. It is built with two connected cylindrical spans of different diameters. Their lengths are 1 m and 0.35 m and their diameters 24 mm and 40 mm, respectively.

4.1. Direct application of the ripple minimization technique

The impedance of the system is known from 1 up to 4000 Hz with a 1 Hz step. The reflection function is first computed with $F_{\max} = 3959\,\text{Hz}$, according to the ripple minimization technique (8) described in section 3.1. As shown on Figure 12, the technique applied in this new geometry does not give the expected result. The two main peaks are not properly described and r_k is beset by ripple. This result is due to the impossibility of f_e matching both propagation times inside the two spans.

4.2. Optimization of two different peaks

The ripple minimization technique is then applied separately to two separated cylindrical ducts of 1 m and 1,35 m

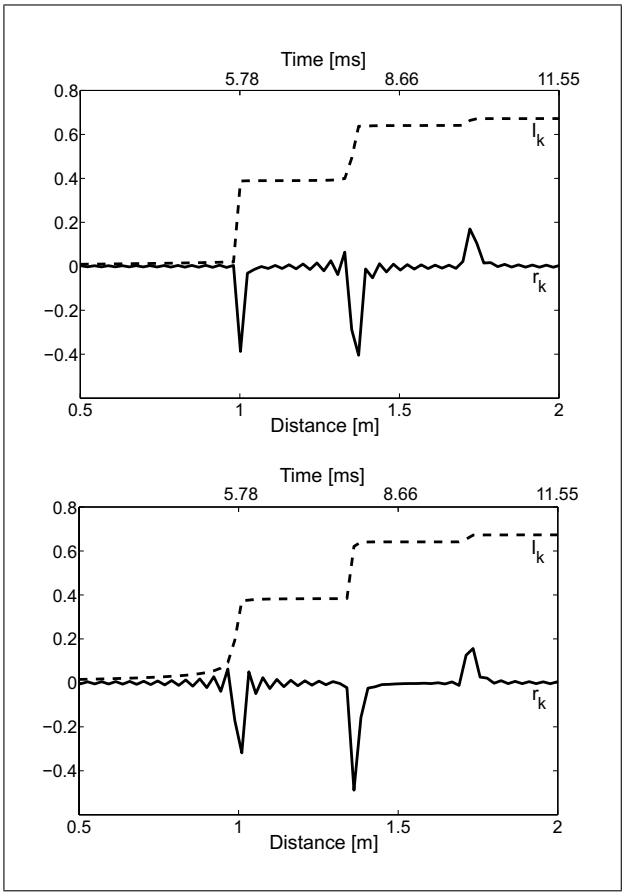


Figure 13. Reflection functions and integrated squared reflection functions of the acoustic line for two different sampling frequencies, top: $\theta(f = F_{\max} = 3974\,\text{Hz}) = 0.80\pi$, bottom: $\theta(f = F_{\max} = 3942\,\text{Hz}) = -0.77\pi$.

in order to optimize the description of the first and the second peak respectively. Two different values of $F_{\max}$ are obtained providing for each separate span a ripple free r_k around the respective maxima (Figure 13).

However, these two different values cause the occurrence of ripple around the other respective peaks. In the first case, the first peak is quite well described with a small amount of ripple, while the second one is beset by ripple (Figure 13a). In the second case, the reflection function (Figure 13b) presents less ripple on the second peak than on the first one. This simple example of two connected tubes of different lengths shows that it is not always possible for the spatial sampling to match all geometrical discontinuities.

These two sampling frequencies associated with the two different $F_{\max}$ (respectively 3974 Hz and 3942 Hz) are fitting the propagation time of the first and the second reflection respectively. The information in the frequency domain only differs by the upper frequency of the domain ($F_{\max}$), the choice having important consequences on the amplitude in the time domain. Phase values on Figure 13 do not exhibit any simple relationship between the phase value of R at $F_{\max}$ and the limitation of the ripple around a specific peak.

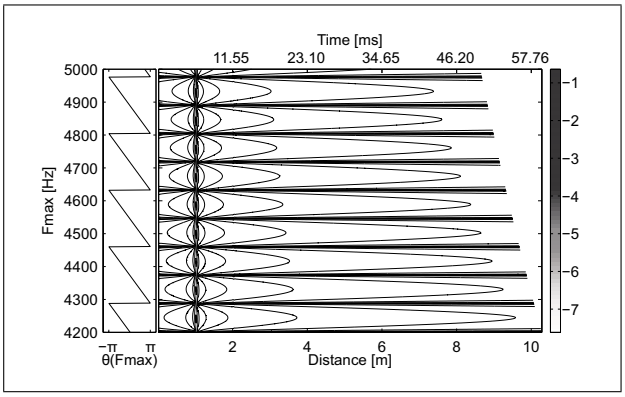


Figure 14. Reflection map for the cylindrical duct (Interval between iso-contour is 0.512).

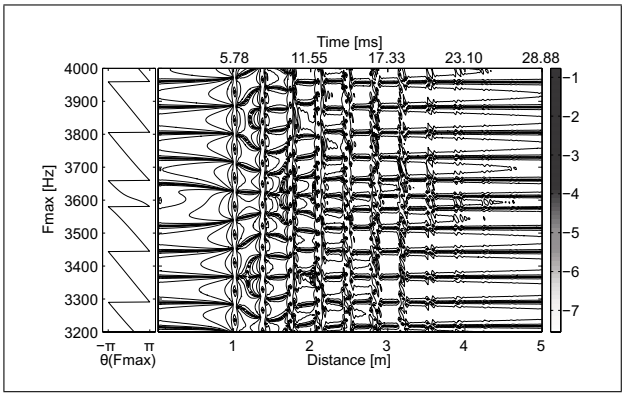


Figure 15. Reflection map for the two-reflection system (Interval between iso-contour is 0.752).

5. The reflection map

5.1. Definition of the reflection map and application to the cylindrical duct

The previous section shows that it is not possible to simultaneously eliminate the ripple on all the peaks in a simple acoustic system built with only tubes of different lengths. A natural extension of the previous example study consists of scanning all the possible values of $F_{\max}$. Reflection functions are computed with the scanned values of $F_{\max}$ (for example the highest 800 values of $F_{\max}$ are scanned). These functions are then differentiated and represented on a 3D plot. The first axis is the sampled time; the second, the whole set of $F_{\max}$ and the third being the amplitude of the differentiated reflection function. Iso-contour lines of their absolute values are then determined and the resulted map is plotted on a 2D graph where the logarithmic amplitude is represented through a grey scale. The abscissa is a sampled time axis while the ordinate is a sampled frequency axis of the different $F_{\max}$. The reflection functions are differentiated in order to emphasize the difference between the variations of the reflection function due to ripple, and the ones due to physics. Moreover, ripple is characterized by a variation, and not by a specific value, of the reflection function.

The reflection map of the 1 m long cylindrical pipe of section 3 presents high values (Figure 14) that are indicating important variations of r_k. If those variations were present for every $F_{\max}$, vertical lines would then appear on the plot. They represent a physical event. If those variations depend on the $F_{\max}$ chosen, they are due to signal processing. The reflection map allows separation of the ripple from the physical events. The vertical lines indicate the position of the physical reflections. For the 1 m long open-end tube, a reflection is expected at 1 m plus the end correction. This end correction is well estimated, at least at low frequency, by $\Delta = 0.6133a$ with a the radius of the tube [12]. It corresponds to a distance of 1.009 m. A zoom in on Figure 14 gives a value between 1 and 1.03 m.

Horizontal lines (when they exist) correspond to a value of $F_{\max}$ that yields a ripple free reflection function. We can check on Figure 14 that the corresponding values of $F_{\max}$ fit the zeros modulo pi of the phase of $R(\omega)$ as predicted in 3.1. The reflection map shows that for $F_{\max} = 4976$ Hz, the result will be free of ripple (solid line on Figure 2). It is also true for 4891 Hz, 4804 Hz and for all the values that correspond to a horizontal line. Those frequency values correspond to real impedances, no matter if they are minima or maxima of the impedance amplitude.

Iso-contour lines, that are neither horizontal nor vertical, correspond to the presence of ripple. For any horizontal straight line plotted on the map that crosses such contours, r_k calculated with the corresponding $F_{\max}$ is beset by ripple. Such is the case with $F_{\max} = 4934$ Hz (dashed line on Figure 2).

To summarize, the most important information of the reflection map hides in the shape of the contour lines. The exact value corresponding to the lines is of secondary importance.

5.2. Application of the reflection map to the two reflections system

The reflection map obtained with the two span system is shown on Figure 15. The vertical lines characterize the two reflections (one at the section discontinuity and one at the end of the tube) and their replicates due to the wave trapped between the discontinuity and the outlet. In section 4.2, the reflection function has been determined for two values of $F_{\max}$, respectively 3974 and 3942 Hz, in order to optimize the description of respectively the first and the second peak (Figure 13). The reflection map does not present a horizontal line for these ordinates. Nevertheless when $F_{\max} = 3974$ Hz, there is a horizontal behaviour of the reflection map around the first peak that leads to a ripple free reflection function around the first peak. However, it is not the case for the second peak at this ordinate. When $F_{\max} = 3942$ Hz, there is a horizontal line around the second peak that leads to a ripple free reflection function around the second peak but beset by ripple around the first one.

A careful examination of the reflection map helps to determine the possibility to minimize the ripple on both peaks. If it appears clearly that there is no solution for a

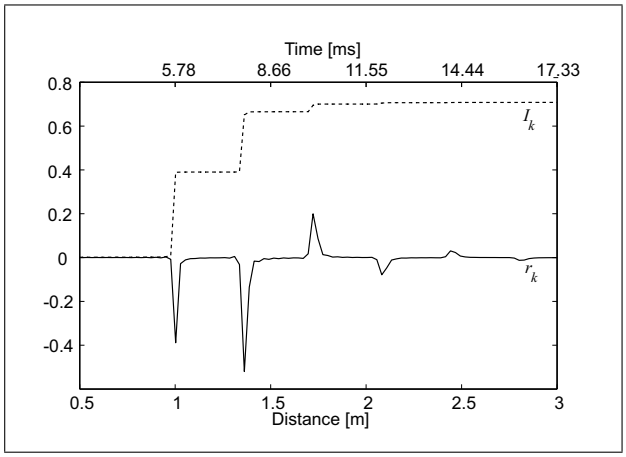


Figure 16. Reflection function and integrated squared reflection function of the two-reflection system for $F_{\max} = 3367$ Hz.

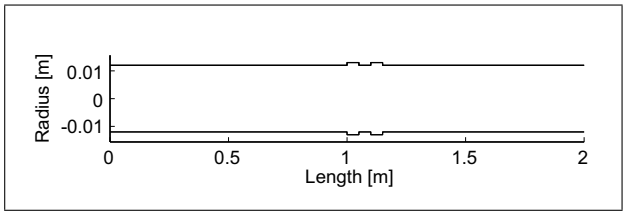


Figure 17. Geometry of the duct. The radius is either 12 or 13 mm at the discontinuities.

ripple free function around both peaks, some values arise as acceptable compromises.

In this particular case, the compromise is excellent for $F_{\max} = 3367$ Hz. The corresponding reflection function is shown on Figure 16. Ripple is very low. With less information in the frequency domain (a lower $F_{\max}$ has been chosen), a better reflection function has been computed, without any filtering or signal processing.

5.3. A more realistic example

The impedance of a complex duct whose geometry is given on Figure 17 allows the reflection function to be calculated. The impedance and the reflection coefficient are shown on Figure 18. The resulting reflection function (Figure 19) is calculated with $F_{\max} = 4900$ Hz.

This tube presents around 1 m four section discontinuities (Figure 17). The lengths of these variations in diameter are 5 cm. As the upper limit of the frequency domain $F_{\max}$ is 4900 Hz, the space sampling Δx_e is 17.7 mm, roughly a third of 5 cm. The reflection function exhibits an important negative peak corresponding to a wave that travels back and forth along 2 m. This negative peak indicates the open end of the tube. High frequency oscillations before and after the peak could be associated with ripple. Around 1 m stronger oscillations that appear periodically (at 3 and 4 m) may be associated with a physical behaviour. Nothing more can be said.

The reflection map (Figure 20) shows not only the event present at 2 m but describes four different events occurring respectively at 1 m, 1.05 m, 1.1 m, and 1.15 m. Hence the

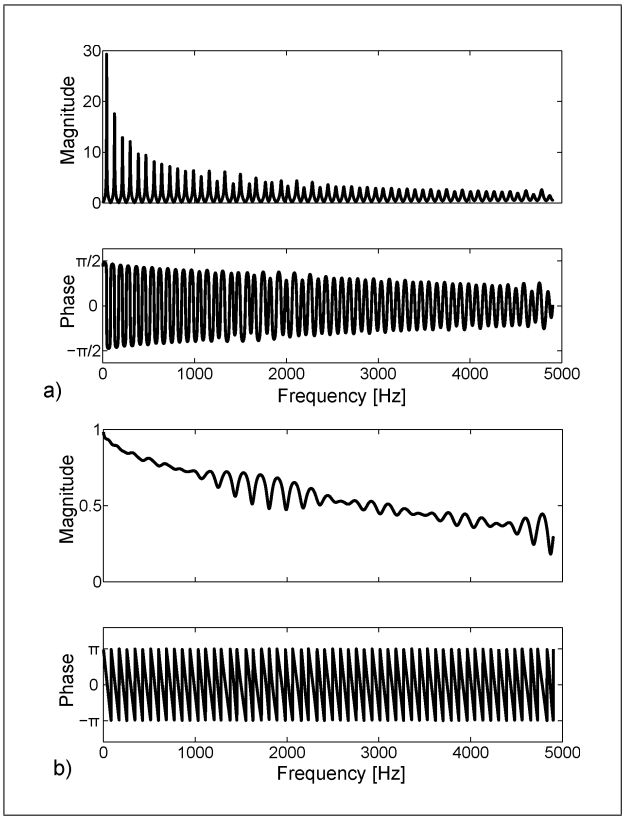


Figure 18. Impedance (a) and corresponding reflection coefficient (b) of the four section discontinuities duct.

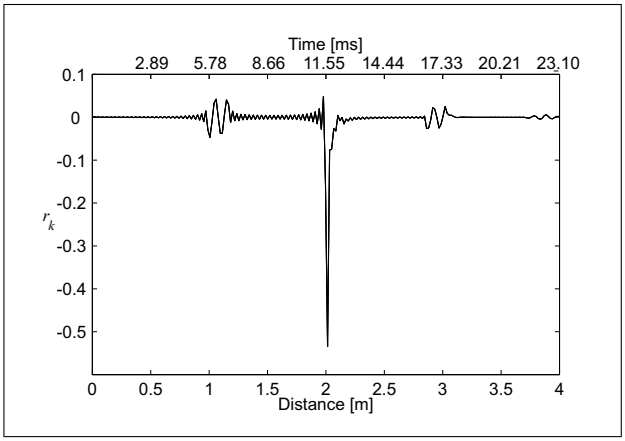


Figure 19. Reflection function of the four section discontinuities duct obtained with $F_{\max} = 4900$ Hz.

corresponding four peaks of the reflection function do represent physical events and are not to be mistaken as ripple. As the sign changes for each event in Figure 19, it is likely the geometry presents a widening at 1 m, a contracting at 1.05 m, a widening at 1.10 m and another contracting at 1.15 m.

The reflection map allows again determination of an $F_{\max}$ minimizing the ripple. An almost horizontal line is present at the ordinate 4434 Hz. The reflection function calculated with $F_{\max} = 4434$ Hz is presented in Figure 21 with the integrated squared reflection function. They are free of ripple.

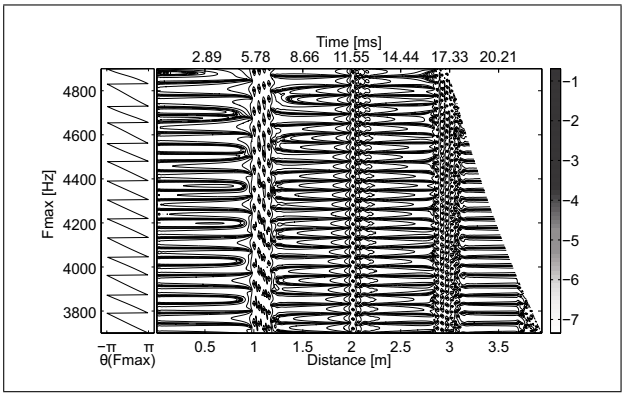


Figure 20. Reflection map of the four section discontinuities duct (Interval between iso-contour is 0.638).

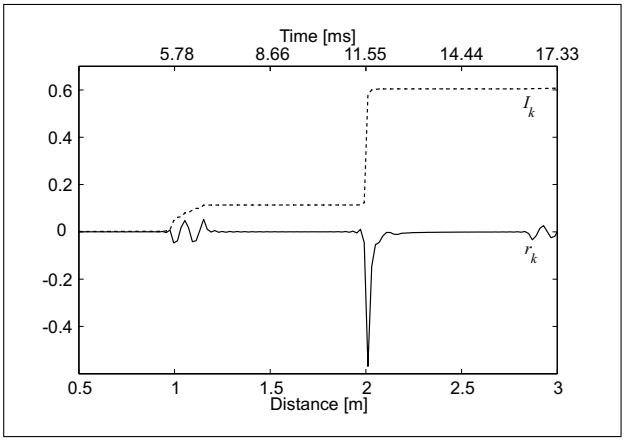


Figure 21. Reflection function and integrated squared reflection function obtained with $F_{\max} = 4434$ Hz.

6. Conclusion

Time domain measurements are often difficult to realize on acoustical real systems, such as engines and musical instruments. Today, frequency domain impedance measurements are of common use. These results allow, through signal processing techniques, determination of time domain dual functions of those obtained in the frequency domain. One of these time domain functions (the reflection function) allows extraction of useful geometrical information, for example in musical synthesis. Unfortunately, the computation of the reflection function from frequency to time domain should involve signal processing bias as well as what is known as ripple. This phenomenon remains present in the integrated squared reflection function that is a new observable, useful to bring to light the discontinuities of the geometry. Because of the ripple, the physical behaviour becomes hidden, and it is often difficult to separate mathematical artefacts from physics with the two latter tools. Instead of extending the integration frequency domain for Fourier Transform, it is possible to optimize the results with a proper choice of the higher frequency of this domain. We can then define a new tool: The reflection map as an indicator of this best choice leading to a ripple free reflection function.

On a cylindrical duct, a trivial solution is always obtained that could match the solution proposed in former papers. On more complicated ducts it is not always possible to find an optimized frequency domain leading to a ripple free reflection function. Nevertheless, compromises are often possible. They minimize the effect of the ripple and allow separation of physical behaviour from signal processing effects in specified time areas.

The reflection map has been of valuable help to determine the integration domain in an example where the discontinuities are near to the limit of resolution imposed by the spatial sampling. It clearly revealed the four discontinuities of the geometry. The reflection function by itself did not give such a result.

References

[1] G. Rosenhouse, N. Amir, U. Shimony: A discrete model for tubular acoustic system with varying cross section. The direct and inverse problems. Part 1: Theory. Acustica **81** (1995) 450–462.

[2] G. Rosenhouse, N. Amir, U. Shimony: A discrete model for tubular acoustic system with varying cross section. The direct and inverse problems. Part 2: Experiments. Acustica **81** (1995) 463–479.

[3] D. Broome: Induction RAM, Part three: Wave phenomena and the design of ram intake systems. Automobile Engineer (1969) June 1969, 262–267.

[4] M. E. McIntyre, R. T. Schumacher, J. Woodhouse: On oscillations of musical instruments. J. Acoust. Soc. Am. **74** (1983) 1325–1345.

[5] B. Gazengel, J. Gilbert, N. Amir: Time domain simulation of single reed wind instrument. From the measured input impedance to the syntthesis signal. Where are the traps? Acta Acustica **3** (1995) 445–472.

[6] N. Amir, U. Shimony: Losses in tubular acoustic systems. Theory and experiment in the sampled time and frequency domain. Acustica united with Acta Acustica **82** (1996) 1–8.

[7] J. D. Polack, X. Meynial, J. Kergomard, C. Cosnard, M. Bruneau: Reflection function of a plane sound wave in a cylindrical tube. Revue de Physique Appliquée **22** (1987) 331–337.

[8] T. Hélié, D. Matignon: Diffusive representations for the analysis and simulation of flared acoustic pipes with viscothermal losses. Mathematical Models and Methods in Applied Sciences **16** (2006) 503–536.

[9] M. Kunt: Traité d'electricité volume XX: Traitement numérique des signaux, section 3.3.4. Presses polytechniques romandes, CH–1015 Lausanne, Switzerland, 1984.

[10] J. Martinez, J. Agullo: Conical bores. Part I: Reflection functions associated with discontinuities. J. Acoust. Soc. Am. **84** (1988) 1613–1619.

[11] R. Caussé, J. Kergomard, X. Lurton: Input impedance of brass musical instruments. Comparison between experiment and numerical models. J. Acoust. Soc. Am. **75** (1983) 241–254.

[12] H. Levine, J. Schwinger: On the radiation of sound from an unflanged circular pipe. Physical Review **73** (1948) 383–406.

[13] V. Gibiat, F. Laloë: Acoustical impedance measurements by the two-microphone-three-calibration (TMTC) method. J. Acoust. Soc. Am. **88** (1990) 2533–2545.

[14] M. Kunt: Traité d'electricité volume XX: Traitement numérique des signaux, section 3.7.7. Presses polytechniques romandes, CH-1015 Lausanne, Switzerland, 1984.